Hindawi
International Journal of Antennas and Propagation
Volume 2020, Article ID 6634050, 10 pages
https://doi.org/10.1155/2020/6634050

Research Article

Radio Propagation Measurements in the Indoor Stairwell Environment at 3.5 and 28 GHz for 5G Wireless Networks

Ahmed Al-Saman, Marshed Mohamed, and Michael Cheffena

The Norwegian University of Science and Technology (NTNU), Innlandet, Gjøvik 2815, Norway

Correspondence should be addressed to Ahmed Al-Saman; ahmed.al-saman@ntnu.no

Received 11 October 2020; Revised 12 November 2020; Accepted 14 December 2020; Published 28 December 2020

Academic Editor: Ana Alejos

To cover the high demand for wireless data services for different applications in the wireless networks, different frequency bands below 6 GHz and in millimeter-wave (mm-Wave) above 24 GHz are proposed for the fifth generation (5G) of communication. The communication network is supposed to handle, among others, indoor traffic in normal situations as well as during emergencies. The stairway is one of those areas which has less network traffic during normal conditions but increases significantly during emergencies. This paper presents the radio propagation in an indoor stairway environment based on wideband measurements in the line of sight (LOS) at two candidate frequencies for 5G wireless networks, namely, 3.5 GHz and 28 GHz. The path loss, root mean square (RMS) delay spread, *K*-factor results, and analysis are provided. The close-in free-space reference distance (CI), floating intercept (FI), and the close-in free-space reference distance with frequency weighting (CIF) path loss models are provided. The channel parameters such as the number of clusters, the ray and cluster arrival rates, and the ray and cluster decay factors are also obtained for both frequencies. The findings of the path loss show that the CI, FI, and CIF models fit the measured data well in both frequencies with the path loss exponent identical to the free-space path loss. Based on clustering results, it is found that the cluster decay rates are identical at both bands. The results from this and previous measurements indicate that at least one access point is required for every two sections of the stairway to support good coverage along the stairwell area in 5G wireless networks. Moreover, for 5G systems utilizing mm-Wave frequency bands, one access point for each stair section might be necessary for increased reliability of the 5G network in stairwell environments.

1. Introduction

The fifth-generation (5G) cellular network evolution is going to exploit the huge available bandwidth in the millimeter-wave (mm-Wave) band and the unoccupied bandwidth in sub-6 GHz. With low latency and huge data rate capacity, the evolution of 5G can lead us to smart, hyperscale haptic Internet-of-Things (IoT) technologies and leverage new types of connectivity such as vehicle-to-infrastructure, vehicle-to-vehicle, vehicle-to-pedestrian, and person-to-person [1]. Ultrahigh-speed and high-efficiency indoor wireless networks are also the future of wireless connectivity in 5G and beyond. The frequency bands in sub-6 GHz (midbands) and a frequency range between 24 and 86 GHz (high bands) have gained increasing attention and now appear to be the most likely candidates to host the upcoming 5G wireless multi-gigabit applications [2, 3].

The radio channel propagation at midbands and high bands can be affected by objects of different sizes due to the variation of the wavelength of the utilized frequencies. The indoor environment represents the rich sources of scattering objects for radio channel propagation. Many structural issues are influencing the indoor radio channel propagation, such as construction materials, building size, and interaction with other systems. All of these obstacles force the signal to propagate across multiple paths through reflection, refraction, and diffraction phenomena.

Many research studies have been conducted in the area of radio channel propagation in various indoor environments such as office [4–6], corridor [7–9], dining room [10],

and laboratory [11] at 28 GHz as the prominent band for 5G wireless networks. Wireless coverage along the stairwell and the understanding of radio spreading in such environments are crucial in enabling the communication of public safety personnel and sharing of information for a swift and effective response.

At low frequencies, many studies have investigated the radio propagation in the stairwell indoor environment [12–18]. The path loss models obtained based on empirical results from measurements at 900 MHz [17], 1800 MHz [19], 2.4 GHz, and 2.8 GHz [13] have high path loss exponents (PLEs) for all frequencies. However, both studies [13, 19] stated that the PLE of the first stair section is less than the free-space path loss (FSPL) due to the existence of the line-of-sight (LOS) path in this section. The LOS path is lost from the next section of the stair onward, and a significant power drop occurs where the power decay, in terms of PLEs, reached up to 12 in some scenarios as presented in [13]. In [14], the wideband measurements using VNA have been conducted in a stair indoor environment at the frequency range of 2.5–2.69 GHz to study the effect of different antenna heights on radio propagation characteristics based on path loss and root mean square (RMS) delay spread.

For high bands, the radio propagation study in indoor stair environments is almost nonexistent. To the best of our knowledge, the only studies which were conducted at high bands in two different stairwells were [20, 21]. The path loss was investigated using different models based on narrowband measurements at 26 GHz, 28 GHz, 32 GHz, and 38 GHz. In this work, the radio propagation characteristics are investigated in a stairwell indoor environment at midbands and high bands based on wideband measurements at 3.5 and 28 GHz with a bandwidth of 2 GHz. The path loss, K-factor, and RMS delay spread are investigated for LOS scenarios in a stairwell indoor environment. The path loss is examined using three different path loss models. The power decay modelling includes the distance and height effects in this work where the height effect is not addressed separately. The channel is characterized at both bands based on the clustering of power delay profile (PDP), and the Saleh–Valenzuela (S-V) model [22] is modified to model the channel in an indoor stair environment at both bands based on measured PDP.

The rest of the paper is organized as follows. The measurement setup and environment are presented in Section 2. The measurement results and analysis are provided in Section 3. The paper is concluded in Section 4.

2. Measurement Campaign

The measurements were conducted in one section of a stairway containing 11 steps in an indoor staircase environment using a vector network analyzer (VNA) connected to transmitter (Tx) and receiver (Rx) antennas. The VNA was configured to measure the S21 parameter in a span (B) of 2 GHz with 2001 frequency points (1 MHz frequency step (Δf)) and central frequencies of 3.5 and 28 GHz, respectively. This measurement configuration results in a maximum resolvable delay of 1 μs ($1/\Delta f$) and a delay resolution of about 0.5 ns ($1/B$). For each center frequency (3.5 and 28 GHz), the Tx antennas were mounted on a tripod 1.7 m above the ground, while the Rx antennas were mounted on a tripod with heights of 1.5 m. The measurement setup parameters are listed in Table 1. Tx was set at a fixed location (top of the stairway), and the S21 parameter was recorded with Rx set at different steps (0, 1, 2, . . ., 10) as depicted in Figure 1.

In this work, the measurement was conducted for the LOS scenario in one section of the stairwell environment. For 3.5 GHz, the omnidirectional antenna was used at Tx and Rx; however, at 28 GHz, the omnidirectional antenna was used at Rx, and the horn antenna was used at Tx. Hence, the Tx antenna needs to be aligned with the Rx antenna in elevation angle. For all steps, it is noticed that the elevation angles for alignment are 27°, 25°, and 23° down tilted for stair steps of 0 to 4, 5 to 9, and 10, respectively. Hence, the elevation angle of the Tx antenna was fixed at 25° for all steps as the middle value between other angles, and the difference was only 2°. In the azimuth plane, Tx aligns 0° with Rx to get the LOS path, and then Tx was rotated with the azimuth half-power beam-width (HPBW) of the antenna of 20° to get all multipath components (MPCs). The processing to get all MPCs as the omnidirectional antenna will be discussed in Section 3.1.

3. Measurement Results

3.1. Power Delay Profile. The PDPs were obtained by finding the square magnitude of the channel impulse responses ($|h_\tau|^2$). The channel impulse responses (h_τ) were obtained by conducting the inverse discrete Fourier transform (IDFT) on the measured transfer function $H(f)$ (S21 parameter). $H(f)$ was filtered by a Hanning window to suppress the undesired side lobes. Figures 2(a) and 2(b) show the PDP at the Tx-Rx separation distance of 2.2 m (step 5 of the stair) for 3.5 and 28 GHz, respectively. The PDP at 3.5 GHz contains all multipath components from all directions as the Tx and Rx antennas are omnidirectional. For 28 GHz, as the directional antenna was used at Tx, the omnidirectional PDP at each Tx-Rx measurement point can be obtained using the synthesized model [23]. Let us define the directional PDP at each Tx angle of i as

$$\mathrm{PDP}_i(\tau) = \left|h_i(\tau)\right|^2. \tag{1}$$

Then, the omnidirectional PDP can be computed as

$$\mathrm{PDP}_{\mathrm{omni}}(\tau) = \max_i \left\{\mathrm{PDP}_i(\tau)\right\}. \tag{2}$$

In our measurements, $\mathrm{PDP}_{\mathrm{omni}}(\tau)$ is collected from seven i angles, namely, 0°, 20°, 40°, −20°, −40°, −60 °, and − 80°. The received signals at the other angles were discarded as they were at the noise level. The resulting omnidirectional PDP $\mathrm{PDP}_{\mathrm{omni}}(\tau)$ at step 5 of the stairs obtained from $\mathrm{PDP}_i(\tau)$ of Figure 2(b) is shown in Figure 3.

Table 1: Measurement setup parameters.

Parameter	Value at 3.5 GHz	Value at 28 GHz
Frequency (GHz)	3.5	28
Bandwidth (GHz)	2	2
Delay resolution (ns)	0.5	0.5
Tx power (dBm)	10	10
Tx antenna type	Omnidirectional	Horn
Rx antenna type	Omnidirectional	Omnidirectional
Tx/Rx polarization	Vertical/vertical	Vertical/vertical
Tx/Rx antenna gain (dBi)	2.5/2.5	18.9/1.5
Tx/Rx antenna azimuth HBPW	—	20°/—
Tx/Rx antenna height (m)	1.7/1.5	1.7/1.5

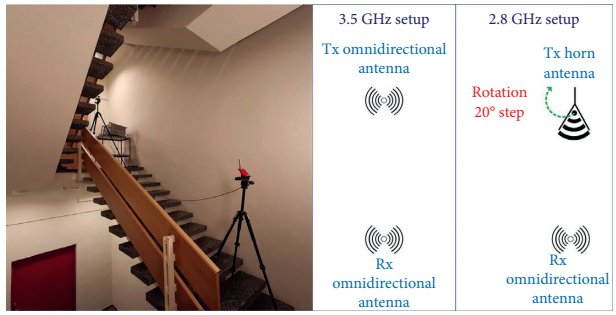

Figure 1: Measurement setup. Tx was fixed at the top of the stair, and Rx was moved along the stair steps.

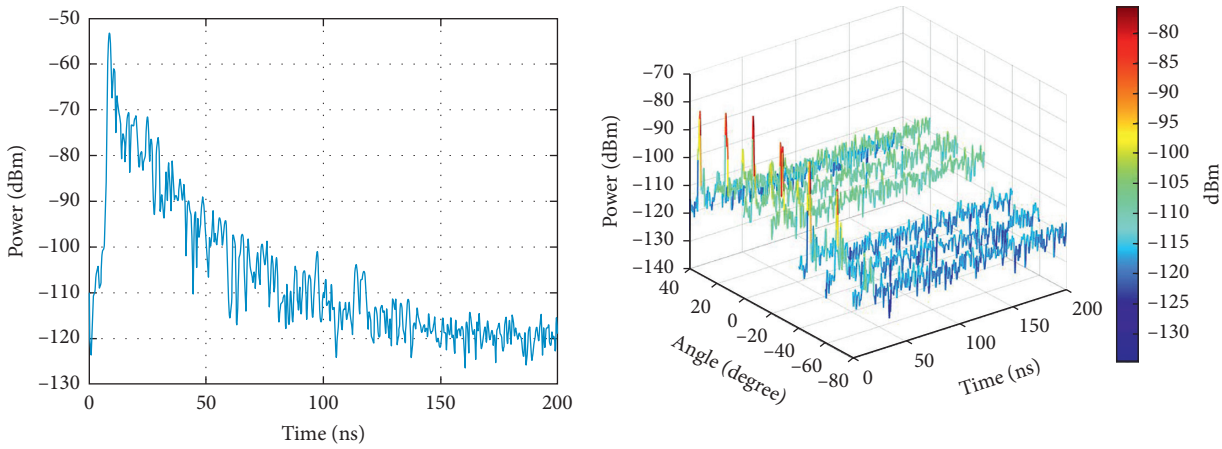

Figure 2: Power delay profile at 2.2 m Tx-Rx separation distance in step 5 of the stair: (a) 3.5 GHz and (b) 28 GHz.

3.2. Path Loss and K-Factor. The path loss (PL) can be calculated from the total sum of the square of the amplitude of the measured paths p_l^2 and the antenna gain as follows [24, 25]:

$$\mathrm{PL}\,(\mathrm{dB}) = -10\log_{10}\left(\frac{\sum_{l=1}^{L} p_l^2}{G_t G_r}\right), \tag{3}$$

where L is the total number of measured paths and G_t and G_r are the gains of the Tx and Rx antennas at the center frequency, respectively. Then, the received power can be calculated as [26]

$$P_r\,(\mathrm{dBm}) = P_t\,(\mathrm{dBm}) - \mathrm{PL}, \tag{4}$$

where P_t is the transmitted power set at 10 dBm for both measured bands.

Figure 4 shows the received power for both bands 3.5 and 28 GHz along with the steps of the stairs. It can be seen that the received power degrades with the stair steps at both bands. It can also be seen that the received power at 28 GHz is less than that of 3.5 GHz by around 20 dBm. To investigate the power decay based on the distance for each frequency, the close-in free-space reference distance (CI) and floating intercept (FI) path loss models were used. Furthermore, the

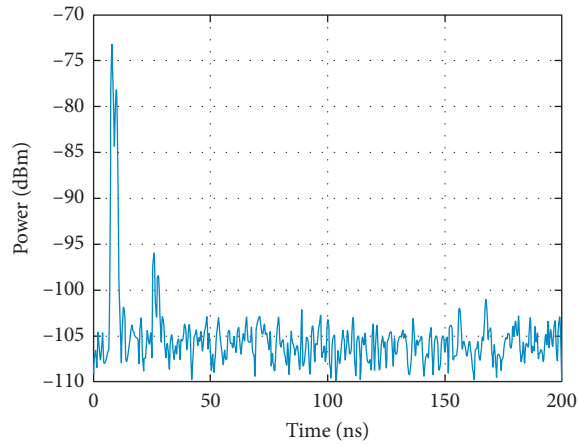

Figure 3: Omnidirectional PDP at 28 GHz in step 5 of the stairs.

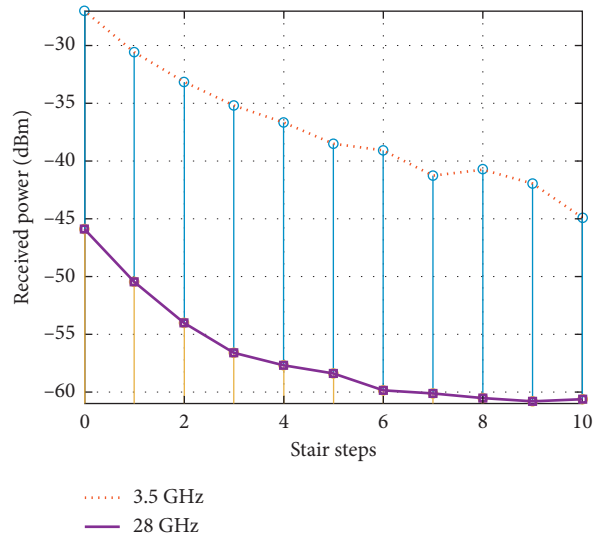

Figure 4: Received power among stair steps at 3.5 GHz and 28 GHz.

close-in free-space reference distance with frequency weighting (CIF) path loss model was used to investigate the power decay based on both distance and frequency.

The CI path loss model can be expressed as

$$\mathrm{PL}^{\mathrm{CI}}(f,d)[\mathrm{dB}] = \mathrm{PL}(f,d_0) + 10n\log_{10}\left(\frac{d}{d_0}\right) + X_\sigma, \quad (5)$$

where $\mathrm{PL}(f,d)$ is the path loss at different frequencies with various Tx-Rx separation distances (d in meters), $\mathrm{PL}(f,d_0)$ is the path loss at a close-in distance d_0 of 1 m or less in dB (in this particular measurement, d_0 is 0.5 m), n denotes the distance dependency of path loss, which is the PLE, and X_σ is a zero-mean Gaussian-distributed random variable with a standard deviation σ (dB) (shadowing effects). The FI path loss model is defined as

$$\mathrm{PL}^{\mathrm{FI}}(d)[\mathrm{dB}] = \alpha + 10.\beta\log_{10}(d) + X_\sigma^{\mathrm{FI}}, \quad (6)$$

where α and β are the floating intercept in dB and the slope of the line, respectively. The shadow fading is represented by zero-mean Gaussian random variable X_σ^{FI} (dB) with a standard deviation of σ (dB).

Figure 5 shows the measured path loss and CI and FI path loss models for both 3.5 and 28 GHz along the stairway. It can be shown that the CI and FI path loss models can fit the measurement data well. From the CI model for both bands, it can be seen that the PLEs are identical with free-space path loss. This means that the LOS path is the dominant path, and the reflected paths have a minor contribution to the overall received power. The CI and FI model parameters are listed in Table 2.

The CIF was recently proposed to model the propagation loss for indoor channels in mm-Wave for the 5G system. It is presented as [4]

$$\mathrm{PL}^{\mathrm{CIF}}(f,d)[\mathrm{dB}] = \mathrm{PL}(f,d_0) + X_\sigma + 10n\left(1 + b\left(\frac{f-f_0}{f_0}\right)\right)\log_{10}\left(\frac{d}{d_0}\right), \quad (7)$$

where n denotes the PLE and b is an optimization parameter that captures the slope or linear frequency dependency of the

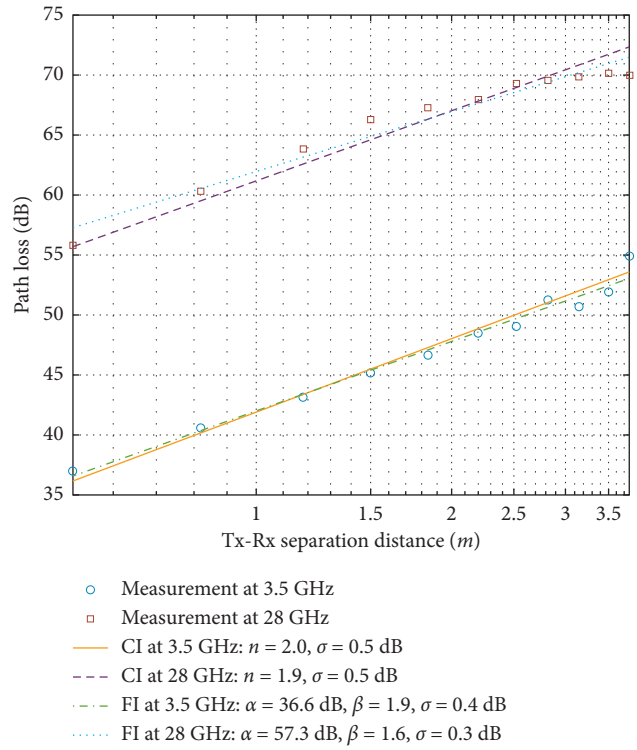

Figure 5: Measured path loss at 3.5 GHz and 28 GHz along stairs compared with CI and FI models.

Table 2: Path loss model parameters.

Frequency (GHz)	Model	PLE for CI β for FI n for CIF	FI (α) (dB)	CIF (b)	σ (dB)
3.5	CI	2	—	—	0.5
	FI	1.9	36.6	—	0.4
	CIF	1.9	—	0.05	0.9
28	CI	1.9	—	—	0.5
	FI	1.6	57.3	—	0.3
	CIF	1.9	—	0.05	0.9

PLE that balances at the centroid of the frequencies being modeled. The term f_0 is a fixed reference frequency, the centroid of all frequencies represented by the path loss model, and serves as the balancing point for the linear frequency dependency of the PLE [4]. It is found as the weighted sum of measurements from different frequencies, using the following equation:

$$f_0 = \frac{\sum_{k=1}^{K} f_k N_K}{\sum_{k=1}^{K} N_K}, \tag{8}$$

where K is the number of unique frequencies and N_k is the number of path loss data points corresponding to the k^{th} frequency f_k. The input parameter f_0 represents the weighted frequencies of all measurement data applied to the model which was calculated using (8), and it was found to be 16 GHz in our measurement.

The CIF path loss model together with the measured data is shown in Figure 6. It can be seen that the CIF model fits the measured data well. The parameters of the CIF model are also listed in Table 2. The PLE value of 1.9 is close to the free-space PLE, and the small value of b indicates that the PLE is not frequency-dependent. This implies that all the frequency-dependent effects are incorporated into the close-in distance d_0 of 0.5 m.

The K-factor of the received signal was also calculated. It represents the ratio of powers between the LOS component and the non-LOS multipath components. Here, the K-factor values were found to be between 3.1 and 5.2 dB and between 2.1 and 7.8 dB at 3.5 and 28 GHz, respectively.

3.3. Delay Spread. The RMS delay spread is generally used to characterize the time dispersion properties of wideband channels. It is a measure of the coherence bandwidth and time dispersion of multipath channels. The square root of the second moment of a PDP represents the RMS delay spread, and it is defined as [27]

$$\tau_{\text{rms}} = \sqrt{\overline{\tau^2} - (\overline{\tau})^2}, \tag{9}$$

where

$$\overline{\tau} = \frac{\sum_l P(\tau_l)\tau_l}{\sum_l P(\tau_l)}, \tag{10}$$

$$\overline{\tau^2} = \frac{\sum_l P(\tau_l)\tau_l^2}{\sum_l P(\tau_l)}. \tag{11}$$

Equations (10) and (11) represent the first moment (mean excess delay) and second central moment of the PDP,

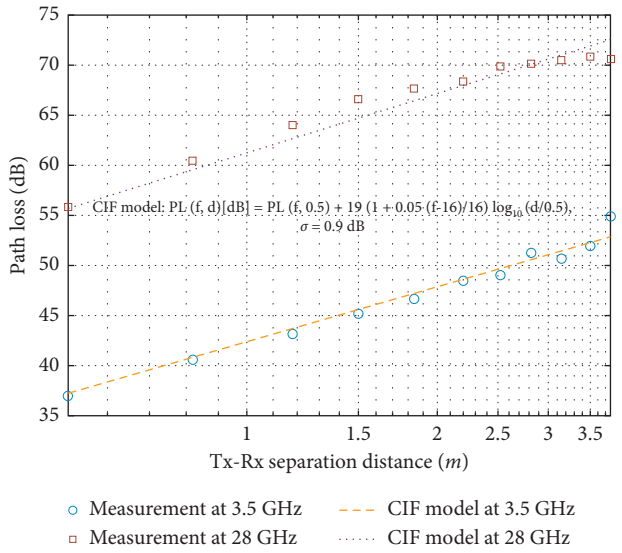

FIGURE 6: CIF path loss model for the measured data for both frequencies.

respectively, and $P(\tau_l)$ is the received power at the l^{th} multipath. The scatter plots of RMS delay spread along the stairway for both bands are shown in Figure 7. It can be seen that the RMS delay spread values are low for both bands and are lower at 28 GHz. This implies that the LOS path contributes to the majority of the received power, and a minor portion of power is from the reflected paths from the wall. The minimum, maximum, and mean values of RMS delay spread are 1.7 ns, 4.9 ns, and 3.5 ns for 3.5 GHz and 0.2 ns, 2.4 ns, and 1.3 ns for 28 GHz.

4. Cluster Identification and Channel Model

The following procedures were performed on the PDP to identify the clusters present in the channel. Firstly, all the peaks in the PDP were identified; however, only the detected peaks above the noise level of 100 dBm were considered as shown in Figure 8. As the measurements are for the LOS scenario, the local maximum before the LOS peak was also discarded. The PDP was then normalized in both power and delay, in which the first cluster starts at 0 ns with a power of 0 dBm. Where there is no void interval in the resulting normalized PDP, visual inspection was used to categorize the normalized PDP into several clusters as shown in Figure 9(a).

The figure shows that the total number of detected paths above the noise threshold at 3.5 GHZ is 31, and the maximum excess delay is 65 ns. The total number of clusters is 3 in which the LOS cluster (first cluster) contains 9 subpaths, and the rest of the multipath components fall in cluster 2 (5 subpaths) and cluster 3 (17 subpaths).

At 28 GHz, where the void intervals between different signal paths are observed, a cluster is then defined as a collection of paths in which the void duration between them is less than 2.5 ns [28].

Based on this clustering method, it is shown in Figure 9(b) that the PDP contains two clusters with two subpaths each, namely, the LOS cluster with a duration of 4 ns and the second cluster of 3.5 ns. The void interval between the two clusters is 14 ns, and the maximum excess delay is 19.5 ns.

Furthermore, the popular model for the indoor channel (S-V model) was used to analyze the measured channel at 3.5 and 28 GHz. The channel impulse response can be modeled using the S-V model as [22]

$$h(\tau) = \sum_{k=1}^{K} \sum_{l=1}^{L_k} g_{lk} e^{j\theta_{lk}} \delta(\tau - T_k - \tau_{lk}), \tag{12}$$

where g_{lk} is the amplitude gain of the l^{th} path in cluster k. T_k and τ_{lk} are the arrival delay of the k^{th} cluster and the relative delay of the l^{th} multipath component in the k^{th} cluster, respectively. K and L_k are the maximum number of clusters and the maximum number of multipath components in the k^{th} cluster, respectively. In the S-V model, the average power gain of the l^{th} multipath component in cluster k is modeled as the double exponential decay of delay:

$$\overline{g_{lk}^2} = \overline{g_{11}^2} e^{-(T_k/\Gamma)} e^{-(\tau_{lk}/\eta)}, \tag{13}$$

where $\overline{g_{11}^2}$ is the average power gain of the first multipath component which is the LOS path in LOS measurement. Γ and η are the cluster and ray power decay constants, respectively. The cluster and rays in the cluster arrive according to the stochastic Poisson process, which leads to the exponential distributions for their interarrival times with Λ and λ cluster and ray arrival rates, respectively. Here, the S-V model is used to describe the channel with four parameters (Γ, η, Λ, and λ). These parameters are extracted from PDP as follows.

4.1. Cluster and Ray Arrival Rates (Λ and λ). The cluster arrival rate (Λ) is determined based on the interarrival times of

$$\Delta T_k = T_k - T_{k-1}. \tag{14}$$

ΔT_k are considered to follow the exponential distribution; hence, the estimated parameter of (Λ) can be obtained based on the maximum likelihood estimator (MLE) as

$$\widehat{\Lambda} = \frac{1}{\overline{\Delta T_k}}, \tag{15}$$

where $\overline{\Delta T_k}$ is the mean of interarrival times (which is the mean of void intervals at 28 GHz in our measurements). In the S-V model, the rays are also assumed to follow the exponential distribution; however, since our delay resolution is 0.5 ns, the IDFT of the measured data cannot resolve the interpath arrival times. This implies that the classical tapped delay-line approach is used to model the ray arrival rate, and each resolved delay bin contains energy according to (13). Hence, each delay tape (ray) arrives at the time interval of 0.5 ns at a rate λ equal to 2 GHz.

Based on our clustering for PDP along with the stair steps, it can be shown that the number of clusters is 3 and 2 in each step for 3.5 and 28 GHz, respectively. For 28 GHz, the

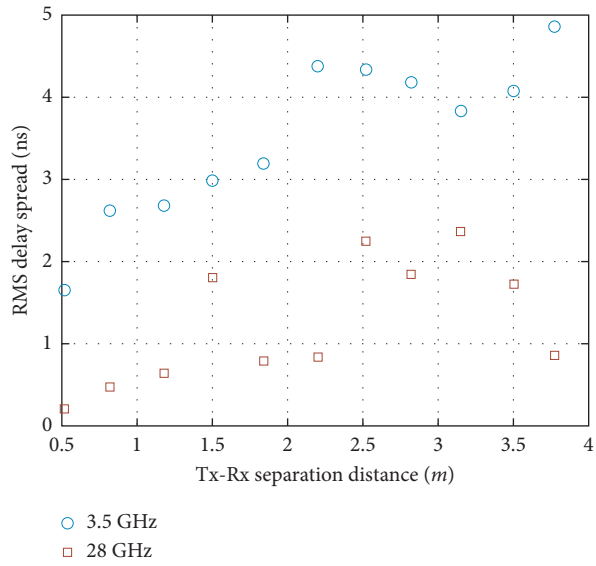

Figure 7: RMS delay spread at 3.5 GHz and 28 GHz.

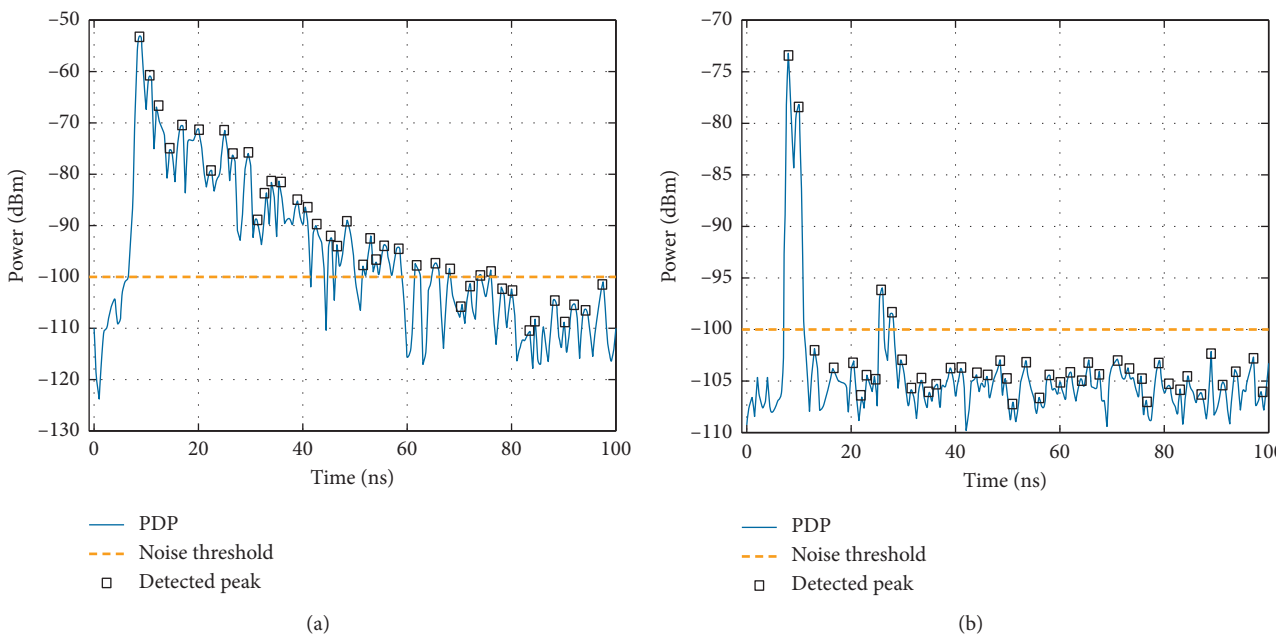

Figure 8: Examples of power delay profile (solid line), noise level (dashed line), and detected peaks (square markers) at 2.2 m Tx-Rx separation distance in step 5 of stairs: (a) 3.5 GHz and (b) 28 GHz.

second cluster for all stair steps has only one path except step 5 that has two paths. For 3.5 GHz, in step 5 of the stair, clusters 2 and 3 have more paths than other stair steps. Hence, the channel realization of step 5 is used to analyze the S-V channel model.

4.2. Cluster and Ray Power Decay (Γ and η). The cluster power decay follows the S-V model (exponentially distributed) in both bands with a cluster power decay constant Γ of 0.3 ns at both bands. The ray power decay η is assumed to be the same for all clusters in the S-V model. However, in this particular indoor scenario, the value of η varies from one cluster to another, and it increases linearly with a cluster arrival time as

$$\eta(T_k) = \eta_1 + c(T_k), \tag{16}$$

where η_1 is the ray power decay constant of the first cluster (LOS cluster). The values of η_1 were found to be 0.3 ns for 3.5 GHz and 0.6 ns for 28 GHz, which result in values of c of 0.15 for 3.5 GHz and 28 GHz. The S-V parameters are listed in Table 3 for both measured bands. It can be seen that the cluster decay rate ($1/\Gamma$) for both bands is the same, and the

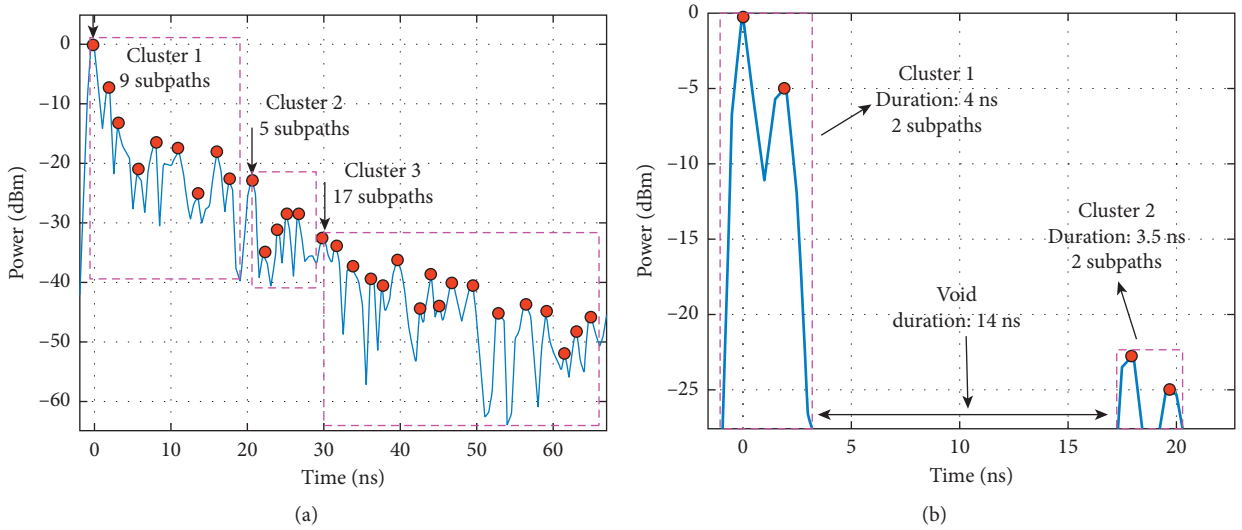

Figure 9: Examples of clustering of measured PDPs for both measured frequencies at 2.2 m Tx-Rx distance (step 5 of the stair): (a) 3.5 GHz and (b) 28 GHz.

Table 3: S-V model parameters.

Frequency (GHz)	$1/\Lambda$ (ns)	$1/\lambda$ (ns)	Γ (ns)	η_1 (ns)	c
3.5	15	0.5	0.3	0.3	0.15
28	14	0.5	0.3	0.6	0.15

ray decay rate for 3.5 GHz is more than the ray decay rate for 28 GHz based on the ray decay rate ($1/\eta_1$) of the power at the first cluster that contains the LOS path.

5. Comparative Study with Related Work

In this section, some previous studies in the indoor stair environment are provided. In [13], the average PLEs along four different stairwells with 5 to 8 stair sections (3 to 12 steps in each stair section) are 8.3 and 9.7 with standard deviations of 5.8 and 7.2 dB at 2.4 and 5.8 GHz, respectively. In [14], based on measurements along 14 stair steps in one stair section at the frequency of 2.5–2.69 GHz, it showed that the PLE is 2.2, and the mean RMS delay spread is 2.8 ns. For high-frequency bands, the works in [20, 21] showed that the PLE values along 10 stair sections with 12 to 13 steps in each stair section are varied from 6.6 to 7.9 with standard deviations from 4.1 to 13.6 dB at 26, 28, 32, and 38 GHz for different antenna polarizations. In our work, the PLEs along 11 stair steps in one stair section are 2 and 1.9 at 3.5 GHz and 28 GHz, respectively, with a standard deviation of 0.5 dB at both bands. The mean RMS delay spreads are 3.5 and 1.2 ns at 3.5 and 28 GHz, respectively.

Based on these conducted measurements on different indoor stair environments for different scenarios, it can be concluded that the path loss for LOS scenarios in the stairwell environment has the same trend of free-space path loss. It indicates that the LOS path is the dominant one where the other reflected rays have less contribution to the total received power in the LOS scenario. In an indoor stairwell environment, the LOS path is only acquired in the first section of the stair; however, for the rest of the sections of the stair, all the paths are contributed from reflected rays. Hence, the PLE is around the FSPL exponent of 2 in one stair section as shown in our work and [14]; however, it is high in the hall stairwell (all sections) as addressed in [13, 20, 21]. This leads us to recommend that, for 5G wireless networks in indoor stairwell environments, at least one access point is needed for every two sections of the stairwell for reliable communication.

6. Conclusion

In this paper, the radio channel characteristics of 3.5 and 28 GHz frequency bands were performed based on LOS indoor measurement results carried out in the stairwell. The S-V model was used to extract the channel parameters from PDP. Based on measurement results, the CI, FI, and CIF path loss models were presented. In general, as expected, the signal experiences more attenuation at a high band of 28 GHz compared to the 3.5 GHz band. The path loss exponents at both frequencies are found close to the FSPL exponent of 2. The RMS delay spread and K-factor were presented. It was found that the RMS delay spreads are low for both frequencies, and it is lower at 28 GHz, indicating that the power is more concentrated around the directed path (LOS path). This is also supported by the large K-factor values with the largest K-factor of 7.8 dB found at 28 GHz. As the multipath components are low, especially at 28 GHz, the number of clusters is less than the clusters at 3.5 GHz. The cluster decay rates are 3.33 at both bands. Based on the LOS cluster (first cluster), it was found that the ray decay rates are 3.33 and 1.7 at 3.5 and 28 GHz, respectively.

Based on this particular measurement and the previously conducted measurements in an indoor stairwell environment, it can be concluded that the LOS scenario can be provided only for the first section of the stair; however, for

the other sections, the received signal was acquired from the reflected paths only (NLOS paths), where the signal degrades more with the increase in the number of sections in the stair. It means that the signal may not be received after two sections of the stair or it is very weak, so to solve this issue, especially for the mm-Wave band of 5G, this study recommends that one access point is needed at every two sections of the stairwell or may be for each section to increase the reliability of the wireless communication system in the stairwell environment that is very important in emergency cases.

Data Availability

The data used to support the findings of this study are available from the corresponding author upon request.

Conflicts of Interest

The authors declare that they have no conflicts of interest.

Acknowledgments

The authors would like to thank Manulab at Norwegian University of Science and Technology, Gjøvik, Norway, for supporting this work.

References

[1] S. Sun, T. S. Rappaport, M. Shafi, P. Tang, J. Zhang, and P. J. Smith, "Propagation models and performance evaluation for 5g millimeter-wave bands," *IEEE Transactions on Vehicular Technology*, vol. 67, no. 9, pp. 8422–8439, 2018.

[2] D. Maisch, "Community concerns over 5g: needless anxiety or wise precaution?" *Chain Reaction*, vol. 136, p. 46, 2019.

[3] T. Jiang, J. Zhang, M. Shafi, L. Tian, and P. Tang, "The comparative study of sv model between 3.5 and 28 GHz in indoor and outdoor scenarios," *IEEE Transactions on Vehicular Technology*, vol. 69, no. 3, pp. 2351–2364, 2019.

[4] G. R. Maccartney, T. S. Rappaport, S. Sun, and S. Deng, "Indoor office wideband millimeter-wave propagation measurements and channel models at 28 and 73 GHz for ultra-dense 5g wireless networks," *IEEE Access*, vol. 3, pp. 2388–2424, 2015.

[5] S. Deng, M. K. Samimi, and T. S. Rappaport, "28 GHz and 73 GHz millimeter-wave indoor propagation measurements and path loss models," in *Proceedings of the 2015 IEEE International Conference on Communication Workshop (ICCW)*, pp. 1244–1250, IEEE, London, UK, July 2015.

[6] M. Lei, J. Zhang, T. Lei, and D. Du, "28-GHz indoor channel measurements and analysis of propagation characteristics," in *Proceedings of the 2014 IEEE 25th Annual International Symposium On Personal, Indoor, and Mobile Radio Communication (PIMRC)*, pp. 208–212, IEEE, Washington, DC, USA, September 2014.

[7] A. M. Al-Samman, T. Abd Rahman, and M. H. Azmi, "Indoor corridor wideband radio propagation measurements and channel models for 5g millimeter wave wireless communications at 19 GHz, 28 GHz, and 38 GHz bands," *Wireless Communications and Mobile Computing*, vol. 2018, Article ID 6369517, 12 pages, 2018.

[8] A. Al-Samman, T. Rahman, M. Azmi, M. Hindia, I. Khan, and E. Hanafi, "Statistical modelling and characterization of experimental mm-wave indoor channels for future 5g wireless communication networks," *PloS One*, vol. 11, no. 9, Article ID e0163034, 2016.

[9] A. M. Al-Samman, T. A. Rahman, T. Al-Hadhrami et al., "Comparative study of indoor propagation model below and above 6 GHz for 5g wireless networks," *Electronics*, vol. 8, no. 1, p. 44, 2019.

[10] A. M. Al-Samman, T. A. Rahman, M. H. Azmi, and S. A. Al-Gailani, "Millimeter-wave propagation measurements and models at 28 GHz and 38 GHz in a dining room for 5g wireless networks," *Measurement*, vol. 130, pp. 71–81, 2018.

[11] X. Wu, Y. Zhang, C.-X. Wang, G. Goussetis, M. M. Alwakeel et al., "28 GHz indoor channel measurements and modelling in laboratory environment using directional antennas," in *Proceedings of the 2015 9th European Conference On Antennas And Propagation (EuCAP)*, pp. 1–5, IEEE, Lisbon, Portugal, April 2015.

[12] S. Y. Lim, Z. Yun, J. M. Baker, N. Celik, H.-s. Youn, and M. F. Iskander, "Propagation modeling and measurement for a multifloor stairwell," *IEEE Antennas and Wireless Propagation Letters*, vol. 8, pp. 583–586, 2009.

[13] S. Y. Lim, Z. Yun, and M. F. Iskander, "Propagation measurement and modeling for indoor stairwells at 2.4 and 5.8 GHz," *IEEE Transactions on Antennas and Propagation*, vol. 62, no. 9, pp. 4754–4761, 2014.

[14] Y. Yu, J. Dong, A.-p. Ye et al., "Effect of antenna height on propagation characteristics under indoor stair environment," in *Proceedings of the 2014 3rd Asia-Pacific Conference On Antennas And Propagation*, pp. 710–712, IEEE, Harbin, China, July 2014.

[15] Y. Yu, Y. Liu, W.-J. Lu, and H.-B. Zhu, "Path loss model with antenna height dependency under indoor stair environment," *International Journal of Antennas and Propagation*, vol. 2014, Article ID 482615, 6 pages, 2014.

[16] P. A. Catherwood and W. G. Scanlon, "Multiple antenna channel characterisation for wearable devices in an indoor stairwell environment," *IET Microwaves, Antennas & Propagation*, vol. 12, no. 6, pp. 920–924, 2017.

[17] O. A. Aziz and T. A. Rahman, "Comparison of indoor propagation models for multi floor staircase at 900 Mhz and 1800 Mhz," in *Proceedings of the 2014 IEEE 2nd International Symposium on Telecommunication Technologies (ISTT)*, pp. 174–178, IEEE, Piscataway, NJ, USA, November 2014.

[18] Y. Wang, X.-L. Wang, Y. Qin, Y. Liu, W.-J. Lu, and H.-B. Zhu, "An empirical path loss model in the indoor stairwell at 2.6 GHz," in *Proceedings of the 2014 IEEE International Wireless Symposium (IWS 2014)*, pp. 1–4, IEEE, Xi'an, China, March 2014.

[19] O. Abdul Aziz and T. A. Rahman, "Investigation of path loss prediction in different multi-floor stairwells at 900 mhz and 1800 mhz," *Progress In Electromagnetics Research M*, vol. 39, pp. 27–39, 2014.

[20] A. M. ALSAMMAN, T. A. Rahman, M. N. HINDIA, and J. Nasir, "Path loss model for indoor emergency stairwell environment at millimeter wave band for 5g network," *Turkish Journal of Electrical Engineering & Computer Sciences*, vol. 26, no. 6, pp. 3024–3032, 2018.

[21] A. O. Aldhaibani, T. A. Rahman, and A. Alwarafy, "Radio-propagation measurements and modeling in indoor stairwells at millimeter-wave bands," *Physical Communication*, vol. 38, Article ID 100955, 2020.

[22] A. A. M. Saleh and R. Valenzuela, "A statistical model for indoor multipath propagation," *IEEE Journal on Selected Areas in Communications*, vol. 5, no. 2, pp. 128–137, 1987.

[23] S. Hur, Y.-J. Cho, J. Lee, N.-G. Kang, J. Park, and H. Benn, "Synchronous channel sounder using horn antenna and indoor measurements on 28 GHz," in *Proceedings of the 2014 IEEE International Black Sea Conference on Communications and Networking (BlackSeaCom)*, pp. 83–87, IEEE, Chisinau, Moldova, May 2014.

[24] A. Karttunen, J. Jarvelainen, A. Khatun, and K. Haneda, "Radio propagation measurements and winner ii parameterization for a shopping mall at 60 ghz," in *Proceedings of the 2015 IEEE 81st Vehicular Technology Conference (VTC Spring)*, pp. 1–5, IEEE, Glasgow, SC, USA, May 2015.

[25] F. Huang, L. Tian, Y. Zheng, and J. Zhang, "Propagation characteristics of indoor radio channel from 3.5 ghz to 28 ghz," in *Proceedings of the 2016 IEEE 84th Vehicular Technology Conference (VTC-Fall)*, pp. 1–5, IEEE, Montréal, Canada, September 2016.

[26] S. R. Saunders and A. Aragï, *Antennas and Propagation for Wireless Communication Systems*, John Wiley & Sons, Hoboken, NJ, USA, 2007.

[27] S. R. Theodore, *Wireless Communications: Principles and Practice*, Prentice-Hall, Upper Saddle River, NJ, USA, 2nd edition, 2002.

[28] T. S. Rappaport, G. R. MacCartney, M. K. Samimi, and S. Sun, "Wideband millimeter-wave propagation measurements and channel models for future wireless communication system design," *IEEE Transactions on Communications*, vol. 63, no. 9, pp. 3029–3056, 2015.